Editorial Manager(tm) JCOMP
Manuscript Draft

Manuscript Number:

Title: Spectral collocation on the unit disc without polar coordinates

Article Type: Regular Article

Keywords: collocation, spectral, unit disc, complex geometry, Poisson problem, Gordon and Hall

Corresponding Author: Dr. Wilhelm Heinrichs Universitat Essen

Other Authors:

Manuscript

SPECTRAL COLLOCATON
on the
UNIT DISC WITHOUT POLAR COORDINATES

by

Wilhelm Heinrichs
Universität Essen, Ingenieurmathematik (FB 10)
Universitätsstr. 3, D-45117 Essen, Germany
E-Mail: wheinric@ing-math.uni-essen.de

Abstract

A new spectral collocation scheme based on the mapping of Gordon and Hall is proposed. Here the unit square is directly mapped onto the unit disc by means of an interpolation technique. Unlike other Poisson solvers on the unit disc no polar coordinates are involved. Hence the usual problems with the pole singularity are avoided. Clearly, the mapping leads to a somewhat larger condition number due to the singularity of the mapping in the four corners of the unit square. Nevertheless we observe the standard high spectral accuracy. This is also shown for more complex geometries. Numerical results are presented which demonstrate the high accuracy of our spectral collocation scheme.

AMS(MOS) classification: 65N35, 65P30, 77C05

Keywords: collocation, spectral, unit disc, complex geometry, Poisson problem, Gordon and Hall.

Figures: 7

Tables: 7

1 Introduction

A new spectral collocation scheme for the Poisson problem on the unit disc is introduced. An efficient Poisson solver is required in many applications, e.g., plasma physics [2], plasma engineering [21], galactic dynamics [3] or gaseous electronics [10, 19, 22]. Also in computational fluid dynamics, a splitting of the Navier–Stokes equations leads to Poisson or "Pseudo-Poisson" problems for the pressure (see [11, 12, 13]). Most Poisson solvers are based on finite difference or finite element methods. Here we consider a spectral collocation scheme.

Spectral methods (see, e.g., Canuto et al. [4] or Gottlieb and Orszag [9, 20]) employ global polynomials for the discretization of elliptic boundary value problems. They give very accurate approximations for smooth solutions with relatively few degrees of freedom. For the collocation scheme it is essential to employ a collocation grid based on Gauss– or Gauss–Lobatto nodes. Hence these methods are well suited for rectangular domains but problems arise for more complex geometries. Since by a stretching any smooth domain can be simply mapped onto the unit disc we consider Poisson problems on this domain. In the previous spectral literature the Poisson equation is transformed into polar coordinates and then solved by means of a combined Chebyshev (or Legendre) and Fourier expansion. Here we refer to the existing papers in [1, 5, 6, 16, 17, 18, 23]. Unfortunately, this transform leads to a coordinate singularity along the axis at the center $r = 0$. Hence most Poisson solvers involve additional "pole conditions" to capture the behaviour of the solution as $r \to 0$. This has been discussed in detail by several authors (see Eisen et al. [6], Huang and Sloan [16] or Shen [23]). An alternative is the use of Gauss-Radau collocation nodes which exclude the center $r = 0$. Hence the singularity at the center is avoided and no extra pole condition is required. The algebraic systems can be efficiently solved by a two-step eigenvalue technique. For a more detailed description we refer to the paper of Chen et al. [5]. Here we use a mapping technique introduced by Gordon and Hall [7, 8] which maps a square into a quadrilateral domain with curved boundaries. In particular, we use this mapping for the unit disc where the curved boundaries are the arcs of the unit circle. Clearly, this mapping has singularities in the four corners which leads to an enlarged condition number of the spectral operator. Due to the boundary conditions the spectral Poisson operator is only evaluated in the inner collocation nodes of the

disc. The large condition number is caused by the collocation nodes next to the four corners. Turning from boundary value problems to time-dependent problems explicit time schemes lead to extremely small time steps. This is typical for singular mappings of this kind. We observed similar problems for the mapping of the square onto the triangle (see [14, 15]). However, the same problem arises for the treatment with polar coordinates where the terms $\frac{1}{r}$ and $\frac{1}{r^2}$ lead to large condition numbers for $r \to 0$. This effect is quite strong since the collocation nodes are dense near the center $r = 0$. Nevertheless we observe the well known high spectral accuracy for the Poisson problem. This is demonstrated by numerical results which are compared to the results of Chen et al. [5], Eisen et al. [6], Huang et al.[16] and Shen [23]. Only in cases where the solution is explicitly given in r (e.g., $u = r^3$) the treatment with polar coordinates yields better results. This is due to the fact that these schemes use expansions in r and the clustering of collocation nodes near $r = 0$. For the other examples we obtain comparable or even better convergence. Hence we found a really striking alternative to the treatment with polar coordinates. This is also confirmed for more complex geometries where we obtain much higher accuracy.

The paper is organized as follows. In the next section we introduce the Poisson problem and the mapping of Gordon and Hall for the unit disc. This is followed by the spectral discretization in section 3. Numerical results and their discussion are presented in section 4. In section 5 we extend this technique to more complex domains.

2 The Poisson Problem and Mapping

We consider the Poisson problem

$$\Delta u = f \ in \ D, \tag{1}$$

$$u = g \ on \ \partial D \tag{2}$$

on the unit disc

$$D = \{(x, y) : \ x^2 + y^2 < 1\}.$$

Here f, g denote given functions defined on D and its boundary ∂D. In order to apply spectral collocation schemes one has to define an transformed

problem on the square. Instead of introducing polar coordinates we prefer the mapping of Gordon and Hall [4, 7, 8]. They found a fairly simple interpolation procedure for mapping a square $Q = (-1,1)^2$ into a quadrilateral with curved boundaries. We first use this mapping technique for mapping Q onto the disc

$$D^* = \sqrt{2}D = \{(x,y):\ x^2 + y^2 < 2\}.$$

The boundary ∂D^* intersects with the four corners of Q. Let the four sides of D^* be denoted by $\Gamma_i,\ i = 1,\ldots,4$ where

$$\begin{aligned}
\Gamma_1 &= \{(x,y):\ y = \sqrt{2-x^2},\ -1 < x < 1\},\\
\Gamma_2 &= \{(x,y):\ x = -\sqrt{2-y^2},\ -1 < y < 1\},\\
\Gamma_3 &= \{(x,y):\ y = -\sqrt{2-x^2},\ -1 < x < 1\},\\
\Gamma_4 &= \{(x,y):\ x = \sqrt{2-y^2},\ -1 < y < 1\}.
\end{aligned}$$

The corresponding sides of the square Q are denoted by $\hat{\Gamma}_i,\ i = 1,\ldots,4$. One uses mappings π_i from $\hat{\Gamma}_i$ to Γ_i to construct the mapping Ψ from Q to D^*. Following Gordon and Hall [4, 7, 8], the mapping Ψ can be expressed in terms of the π_i as follows:

$$\begin{aligned}
\Psi(\xi,\eta) &= \frac{1-\eta}{2}\pi_3(\xi) + \frac{1+\eta}{2}\pi_1(\xi)\\
&+ \frac{1-\xi}{2}\left[\pi_2(\eta) - \frac{1+\eta}{2}\pi_2(1) - \frac{1-\eta}{2}\pi_2(-1)\right]\\
&+ \frac{1+\xi}{2}\left[\pi_4(\eta) - \frac{1+\eta}{2}\pi_4(1) - \frac{1-\eta}{2}\pi_4(-1)\right].
\end{aligned}$$

The functions $\pi_i,\ i = 1,\ldots,4$ are now explicitly given by

$$\pi_1(\xi) = \begin{pmatrix} \xi \\ \sqrt{2-\xi^2} \end{pmatrix},\quad \pi_3(\xi) = \begin{pmatrix} \xi \\ -\sqrt{2-\xi^2} \end{pmatrix},\ -1 < \xi < 1,$$
$$\pi_2(\eta) = \begin{pmatrix} -\sqrt{2-\eta^2} \\ \eta \end{pmatrix},\quad \pi_4(\eta) = \begin{pmatrix} \sqrt{2-\eta^2} \\ \eta \end{pmatrix},\ -1 < \eta < 1.$$

This defines the mapping of Q onto D^*. Finally one obtains D by the stretching

$$(x,y) \ \rightarrow\ (x,y)/\sqrt{2}.$$

Since we are interested in the solution of the Poisson problem we have to transform the Laplace operator into the coordinates of Q. The coordinates (x, y) of D are considered as a function of the coordinates of Q, i.e., $x = x(\xi, \eta),\ y = y(\xi, \eta)$. The partial derivatives are now transformed as follows:

$$\begin{bmatrix} x_\xi & y_\xi & 0 & 0 & 0 \\ x_\eta & y_\eta & 0 & 0 & 0 \\ x_{\xi\xi} & y_{\xi\xi} & x_\xi^2 & 2x_\xi y_\xi & y_\xi^2 \\ x_{\xi\eta} & y_{\xi\eta} & x_\xi x_\eta & x_\xi y_\eta + x_\eta y_\xi & y_\xi y_\eta \\ x_{\eta\eta} & y_{\eta\eta} & x_\eta^2 & 2x_\eta y_\eta & y_\eta^2 \end{bmatrix} \begin{bmatrix} u_x \\ u_y \\ u_{xx} \\ u_{xy} \\ u_{yy} \end{bmatrix} = \begin{bmatrix} u_\xi \\ u_\eta \\ u_{\xi\xi} \\ u_{\xi\eta} \\ u_{\eta\eta} \end{bmatrix}. \tag{3}$$

By inverting the above matrix and taking the sum of the third and fifth row we exactly obtain the coefficients of the transformed Laplace operator in (ξ, η) coordinates. Now we are able to apply spectral collocation schemes.

3 Spectral collocation

On Q we employ the standard Chebyshev Gauss–Lobatto collocation nodes given by

$$(\xi_i, \eta_j) = (\cos\frac{i\pi}{N}, \cos\frac{j\pi}{N}),\ i, j = 0, \ldots, N.$$

By using the described mapping technique of Gordon and Hall we map these collocation nodes onto the disc D. For $N = 24$ they are plotted in Figure I. Clearly, they are clustering near the points $(x, y) = (\pm 1/\sqrt{2}, \pm 1/\sqrt{2})$ on which the four corners are mapped. A zoom of the collocation nodes near $(x, y) = (1/\sqrt{2}, 1/\sqrt{2})$ is presented in Figure II. The above partial derivatives of x, y and u in ξ, η are derived by means of the spectral collocation operators. In the following we write the spectral derivatives in matrix notation. First one has to introduce the transformation matrices from physical space to coefficient space. Since we employ a Chebyshev expansion we obtain the following matrix:

$$T \;=\; \left(\cos(k\frac{i\pi}{N})\right),\ i, k = 0, \ldots, N.$$

Further we need the differentation matrix in the Chebyshev coefficient space which is explicitly given by $\hat{D} = (d_{i,j}) \in \mathbb{R}^{N+1,N+1}$ with

$$d_{i,j} \;=\; \begin{cases} \frac{2j}{c_i},\; j = i+1, i+3, \ldots, N \\ 0\,, \qquad\qquad \text{else} \end{cases}$$

and

$$c_i \;=\; \begin{cases} 2,\; i = 0, \\ 1,\;\; \text{else.} \end{cases}$$

Now we are able to write the spectral derivative matrices $D1$ and $D2$ for the first and second derivatives. They are explicitly given by

$$D1 = T\hat{D}T^{-1},\;\; D2 = T\hat{D}^2T^{-1}.$$

The spectral operators can be efficiently evaluated by Fast Fourier Transforms (FFTs) in $O(N \log N)$ arithmetic operations. We further introduce the identity matrix $I \in \mathbb{R}^{N+1,N+1}$. By tensor product representation

$$A \otimes B = (Ab_{i,j})_{i,j}$$

we are now able to write the spectral derivatives in 2D. The first order partial derivatives are given by

$$\frac{\partial}{\partial \xi} \cong D1 \otimes I,\;\; \frac{\partial}{\partial \eta} \cong I \otimes D1.$$

The second order derivatives are defined by

$$\frac{\partial^2}{\partial \xi \partial \xi} \cong D2 \otimes I,\;\; \frac{\partial^2}{\partial \xi \partial \eta} \cong D1 \otimes D1,\;\; \frac{\partial^2}{\partial \eta \partial \eta} \cong I \otimes D2.$$

The 2D spectral operators can be efficiently evaluated by FFTs in $O(N^2 \log N)$ arithmetic operations. Now it is an easy task to implement the collocation scheme.

4 Numerical Results

Due to the singularity of the above mapping ("corners are mapped onto the smooth parts of the circle") a large condition number can be expected. In table I, we compared the condition numbers of the spectral Laplacian on D

and Q. They are numerically evaluated in the spectral norm and are denoted by

$$cond_2^D,\ cond_2^Q.$$

From the numerical results we observe that the condition number on D is about 2-3 digits larger than on Q. For time-dependent problems this leads to prohibitively small time steps which is typical for such kind of singular mappings. Here we recommend implicit time schemes. However, we consider stationary problems and are interested in the global accuracy of the method. For this purpose we calculated the discrete L^∞ and L^2 - errors on D. They are denoted by E_∞^D and E_2^D where

$$E_\infty^D = \max\{|(u-u_N)(x_i,y_j)| :\ i,j=0,\ldots,N\}$$

and

$$E_2^D = \frac{1}{N}\sqrt{\sum_{i,j=0}^{N}(u-u_N)^2(x_i,y_j)}.$$

The errors are once more compared to the corresponding results on Q which are denoted by E_∞^Q, E_2^Q. We consider an example (see [5, 6, 16]) with a smooth solution given by

$$u(x,y) = \cos(7y+8x+0.7). \tag{4}$$

From table II we observe that the large condition number does not disturb the high spectral accuracy. The results on Q are only slightly better than on D. For $N=28$ the precision of our machine (double precision) is already achieved. Hence the singularity of the mapping has nearly no influence on the accuracy. We further compared our method to the other schemes based on polar coordinates (see [5, 6, 16, 23]). Here we have to notice that the cited references take

$$N_r = N,\ N_\theta = 2N$$

for the polar coordinates (r,θ). Hence they employ $2N^2$ degrees of freedom whereas our method only requires N^2 degrees of freedom. For a fair compare with the cited results with $N=8$ we here take $N=12$. The error is measured in the L^∞ – norm. We present numerical results for the above example and

$$u(x,y) = e^{x+y} \tag{5}$$

$$u(x,y) = (x^2+y^2)^{3/2} \tag{6}$$

$$u(x,y) = (x^2+y^2)^2. \tag{7}$$

For example (4) we obtain better results than the other references. For example (5) our results are similar to the others whereas for the examples (6),(7) we obtain much worse results. In the last examples the exact solutions $u = r^3, r^4$ can explicitly be written in r and hence the polar coordinate approaches yield exact results (up to machine precision). Due to the singularity of the solution in cartesian coordinates the spectral accuracy of our method is disturbed. Clearly, for problems where the solution is an algebraic polynomial in r or a trigonometric polynomial in θ the other approaches have better approximation properties. But in general our scheme is comparable or even better than the methods with polar coordinates.

5 Complex geometry

Here we apply the mapping technique of Gordon and Hall to more complex geometries. We consider the Poisson problem on domains with smooth boundaries Γ which are parameterized in the arc length θ:

$$\Gamma(\theta) = \begin{pmatrix} d(\theta)\cos(\theta) \\ d(\theta)\sin(\theta) \end{pmatrix}, \ 0 \leq \theta < 2\pi.$$

Here $d(\theta)$ denotes the radius in θ. The domain is normalized such that $d(\pi/4) = 1$. In order to apply the mapping technique of Gordon and Hall we have to define the mappings $\pi_i, \ i = 1, 2, 3, 4$. Here we only consider π_1. For given $\xi_j = \cos(j\pi/N), \ j = 0, \ldots, N$ one determines the arc length θ_j by solving the equation

$$d(\theta)\cos(\theta) = \xi_j$$

by a few steps of a Newton iteration. Then we obtain

$$\pi_1(\xi_j) = \begin{pmatrix} \xi_j \\ d(\theta_j)\sin(\theta_j) \end{pmatrix}. \tag{8}$$

A similar technique works for the other three mappings.

Since the boundary curve is already given in a parameterized form it makes sense to define modified mappings $\hat{\pi}_i$ in the arc length θ. We once more describe this approach only for $\hat{\pi}_1$. First one maps the variable $\xi \in [-1, 1]$ onto $\theta \in [\pi/4, 3\pi/4]$ by

$$\theta = \theta(\xi) = \frac{\pi}{4}(2 - \xi).$$

Then for given ξ_j we determine $\theta_j = \theta(\xi_j)$ and obtain

$$\hat{\pi}_1(\xi_j) = \begin{pmatrix} d(\theta_j)\cos(\theta_j) \\ d(\theta_j)\sin(\theta_j) \end{pmatrix}. \tag{9}$$

A similar approach works on the other three parts of the boundary. By a numerical simulation we compared both approaches. We consider boundary curves given by

$$\hat{d}(\theta) = 1 + \sin^2(k\theta), \quad k = 0, 1, 2 \tag{10}$$

which are normalized such that $d(\pi/4) = 1$, i.e.,

$$d(\theta) = \hat{d}(\theta)/\hat{d}(\frac{\pi}{4}), \quad k = 0, 1, 2.$$

For $k = 0$ we reobtain the unit disc and for $k = 1, 2$ the boundaries become more complex. In the figures III,IV we plotted the distribution of collocation nodes for $k = 1, 2$ due to the parameterized mapping (9). We numerically calculated the discrete L^2–error for the Poisson problem with the exact solutions (4),(5). The errors are denoted by E_2 for mapping (8) and E_2^p for the parameterized mapping (9). The corresponding results are presented in the tables IV,V for $k = 0, 1, 2$. On the unit disc ($k = 0$) mapping (8) yields most favorite results. For more complex domains ($k = 1, 2$) the parameterized version (9) becomes more accurate. This could be expected since a discretization along the arc length yields a higher order resolution of the boundary. Clearly, for increasing k the spectral accuracy is somewhat disturbed. For $k \geq 3$ the collocation nodes near the four corners are mapped onto nodes outside the domain (see figure V). Hence for increasing oscillations of the boundary the present approach is no more suitable. But for moderate oscillations of the boundary curve we obtained a high order method.

For more complex domains we also tested the polar coordinate approach. The mapping is given by

$$\begin{pmatrix} x \\ y \end{pmatrix} = r \begin{pmatrix} d(\theta)\cos(\theta) \\ d(\theta)\sin(\theta) \end{pmatrix}, \ 0 \leq r \leq 1, \ 0 \leq \theta < 2\pi. \tag{11}$$

We have to transform the Laplace operator into the polar coordinates. For this purpose we introduce the following abbreviations:

$$d = d(\theta), \ d' = d'(\theta), \ d'' = d''(\theta), \ c = \cos(\theta), \ s = \sin(\theta).$$

The partial derivatives are now transformed as follows:

$$\begin{bmatrix} a_{11} & a_{12} & a_{13} & 0 & 0 \\ a_{21} & a_{22} & a_{23} & 0 & 0 \\ a_{31} & a_{32} & a_{33} & a_{34} & a_{35} \\ 0 & 0 & 0 & a_{44} & a_{45} \\ 0 & 0 & 0 & a_{54} & a_{55} \end{bmatrix} \begin{bmatrix} u_{xx} \\ u_{xy} \\ u_{yy} \\ u_x/r \\ u_y/r \end{bmatrix} = \begin{bmatrix} u_{rr} \\ (ru_{r\theta} - u_\theta)/r^2 \\ u_{\theta\theta}/r^2 \\ u_r/r \\ u_\theta/r^2 \end{bmatrix} \tag{12}$$

where $A = (a_{ij}),\ i,j = 1,2,3$ is given by

$$A = \begin{bmatrix} d^2c^2 & 2csd^2 & d^2s^2 \\ dc(d'c - ds) & d^2(c^2 - s^2) + 2dd'cs & ds(d's + dc) \\ (d'c - ds)^2 & 2(d'^2 - d^2)sc + 2dd'(c^2 - s^2) & (d's + dc)^2 \end{bmatrix}$$

and the other components are

$$\begin{aligned} a_{34} &= d''c - 2d's - dc,\ a_{35} = d''s + 2d'c - ds, \\ a_{44} &= dc,\ a_{45} = ds,\ a_{54} = d'c - ds,\ a_{55} = d's + dc. \end{aligned}$$

By inverting the above matrix and taking the sum of the first and third row we exactly obtain the coefficients of the transformed Laplace operator in polar coordinates. Now we are able to apply spectral collocation schemes. Here we follow the approach of Chen et al. [5]. In the radius r they employ Chebyshev Gauss–Radau collocation nodes given by

$$r_j = \frac{1}{2}\left(1 + \cos\frac{2\pi j}{2N_r + 1}\right),\ j = 0, \ldots, N_r.$$

The center $r = 0$ is avoided and hence no extra pole condition is required. The corresponding transformation matrix T now results in

$$T = \left(\cos\frac{2\pi jk}{2N_r + 1}\right),\ j,k = 0, \ldots, N_r.$$

The derivatives in r can be constructed in the same way as in section 3. The derivatives in θ are obtained by Fourier collocation (see [4]). The collocation nodes are equidistant, i.e.,

$$\theta_j = \frac{2\pi j}{N_\theta},\ j = 0, \ldots, N_\theta - 1.$$

The derivative matrix is explicitly given by

$$(D_{N_\theta})_{kj} = \begin{cases} \frac{1}{2}(-1)^{k+j} \cot \frac{(k-j)\pi}{N_\theta}, & k \neq j \\ 0 & , k = j. \end{cases}$$

Partial derivatives are derived by tensor product representation. In our applications we choose

$$N_r = N, \quad N_\theta = 2N.$$

We performed numerical simulations for the examples (4) and (5). The errors in the discrete L^2- and L^∞ – norms were calculated. The boundary curve is once more given by (10) with $k = 1, 2, 3$. Here we observe that also for increasing k we obtain reasonable distributions of collocation nodes (see figures VI,VII for $k = 2, 3$ and $N = 16$). Clearly, due to the high oscillation of the solution we obtain less favorable results for example (4) (see table VI). Here the mapping of Gordon and Hall yields much better results. The difference between polar coordinates and our mapping technique becomes more striking for example (5) (see table VII). For $N = 32$ we always obtain machine accuracy with an error of about 10^{-14}. For increasing complexity of the domain ($k \geq 3$) we recommend a decomposition of the domain so that on each subdomain the proposed mapping technique can be employed.

CONCLUSION

Poisson problems on the unit disc are solved by spectral collocation schemes based on the mapping of Gordon and Hall. The problems of polar coordinate approaches with pole singularities are avoided and the well known high spectral accuracy is maintained. Due to the corner singularity of the transform we obtain large condition numbers which lead to extremely small time step restrictions for explicit time discretizations. For a compare we present numerical results which show the good performance of our new approach. Finally it is shown that the method can be successfully applied to more complex domains.

TABLES

N	$cond_2^D$	$cond_2^Q$
4	$1.16 \cdot 10^1$	$8.16 \cdot 10^0$
8	$1.07 \cdot 10^3$	$8.92 \cdot 10^1$
12	$2.32 \cdot 10^4$	$4.25 \cdot 10^2$
16	$2.19 \cdot 10^5$	$1.32 \cdot 10^3$
20	$1.27 \cdot 10^6$	$3.19 \cdot 10^3$
24	$5.38 \cdot 10^6$	$6.59 \cdot 10^3$
28	$1.83 \cdot 10^7$	$1.22 \cdot 10^4$
32	$5.30 \cdot 10^7$	$2.07 \cdot 10^4$

Table I. Condition numbers on D and Q.

N	E_2^D	E_∞^D	E_2^Q	E_∞^Q
4	$5.12 \cdot 10^0$	$1.49 \cdot 10^1$	$6.76 \cdot 10^0$	$1.79 \cdot 10^1$
8	$8.73 \cdot 10^{-2}$	$2.38 \cdot 10^{-1}$	$7.02 \cdot 10^{-2}$	$1.53 \cdot 10^{-1}$
12	$1.73 \cdot 10^{-3}$	$6.97 \cdot 10^{-3}$	$8.76 \cdot 10^{-4}$	$2.04 \cdot 10^{-3}$
16	$7.81 \cdot 10^{-6}$	$2.73 \cdot 10^{-5}$	$3.44 \cdot 10^{-6}$	$9.37 \cdot 10^{-6}$
20	$1.44 \cdot 10^{-8}$	$4.80 \cdot 10^{-8}$	$5.44 \cdot 10^{-9}$	$1.60 \cdot 10^{-8}$
24	$1.60 \cdot 10^{-11}$	$5.45 \cdot 10^{-11}$	$4.12 \cdot 10^{-12}$	$1.28 \cdot 10^{-11}$
28	$2.35 \cdot 10^{-13}$	$8.39 \cdot 10^{-13}$	$1.28 \cdot 10^{-14}$	$6.38 \cdot 10^{-14}$
32	$2.10 \cdot 10^{-13}$	$9.37 \cdot 10^{-13}$	$2.00 \cdot 10^{-14}$	$7.21 \cdot 10^{-14}$

Table II. Numerical results for example (4).

Example	Present	Chen [5]	Eisen [6]	Huang [16]	Shen [23]
$\cos(7x+8y+0.7)$	$6.97{\cdot}10^{-3}$	$3.96{\cdot}10^{-1}$	$1.47{\cdot}10^{0}$	$4.11{\cdot}10^{-1}$	$--$
e^{x+y}	$3.87{\cdot}10^{-7}$	$2.72{\cdot}10^{-8}$	$3.27{\cdot}10^{-6}$	$2.61{\cdot}10^{-8}$	$2.6{\cdot}10^{-8}$
$r^3=(x^2+y^2)^{3/2}$	$1.48{\cdot}10^{-2}$	$6.38{\cdot}10^{-16}$	$2.92{\cdot}10^{-2}$	$3.55{\cdot}10^{-14}$	$3.8{\cdot}10^{-16}$
$r^4=(x^2+y^2)^2$	$8.28{\cdot}10^{-7}$	$8.63{\cdot}10^{-15}$	$--$	$3.30{\cdot}10^{-14}$	$--$

Table III. Numerical results for examples (4–7).

	$k=0$		$k=1$		$k=2$	
N	E_2	E_2^p	E_2	E_2^p	E_2	E_2^p
8	$8.73{\cdot}10^{-2}$	$1.36{\cdot}10^{-1}$	$2.08{\cdot}10^{-1}$	$2.08{\cdot}10^{-1}$	$3.25{\cdot}10^{-1}$	$2.35{\cdot}10^{-1}$
16	$7.81{\cdot}10^{-6}$	$9.77{\cdot}10^{-5}$	$1.25{\cdot}10^{-3}$	$3.13{\cdot}10^{-3}$	$3.03{\cdot}10^{-2}$	$3.89{\cdot}10^{-3}$
24	$1.60{\cdot}10^{-11}$	$8.23{\cdot}10^{-9}$	$5.10{\cdot}10^{-5}$	$1.12{\cdot}10^{-5}$	$3.59{\cdot}10^{-3}$	$3.79{\cdot}10^{-5}$
32	$2.10{\cdot}10^{-13}$	$2.99{\cdot}10^{-13}$	$4.15{\cdot}10^{-6}$	$1.68{\cdot}10^{-8}$	$5.08{\cdot}10^{-4}$	$2.77{\cdot}10^{-7}$

Table IV. Numerical results for example (4) with Gordon and Hall.

	$k=0$		$k=1$		$k=2$	
N	E_2	E_2^p	E_2	E_2^p	E_2	E_2^p
8	$8.58{\cdot}10^{-6}$	$1.26{\cdot}10^{-6}$	$9.30{\cdot}10^{-4}$	$1.78{\cdot}10^{-4}$	$4.25{\cdot}10^{-3}$	$1.93{\cdot}10^{-3}$
16	$1.71{\cdot}10^{-9}$	$1.14{\cdot}10^{-12}$	$3.69{\cdot}10^{-5}$	$7.91{\cdot}10^{-9}$	$4.66{\cdot}10^{-4}$	$3.61{\cdot}10^{-7}$
24	$5.47{\cdot}10^{-13}$	$4.84{\cdot}10^{-14}$	$2.65{\cdot}10^{-6}$	$4.51{\cdot}10^{-13}$	$5.98{\cdot}10^{-5}$	$1.33{\cdot}10^{-10}$
32	$8.22{\cdot}10^{-14}$	$9.65{\cdot}10^{-14}$	$2.33{\cdot}10^{-7}$	$7.89{\cdot}10^{-14}$	$8.63{\cdot}10^{-6}$	$8.73{\cdot}10^{-14}$

Table V. Numerical results for example (5) with Gordon and Hall.

	$k=1$		$k=2$		$k=3$	
N	E_2	E_∞	E_2	E_∞	E_2	E_∞
8	$1.91\cdot10^{0}$	$2.82\cdot10^{0}$	$2.58\cdot10^{0}$	$4.99\cdot10^{0}$	$1.14\cdot10^{0}$	$2.34\cdot10^{0}$
16	$5.81\cdot10^{-2}$	$1.46\cdot10^{-1}$	$3.09\cdot10^{-1}$	$5.93\cdot10^{-1}$	$4.29\cdot10^{-1}$	$1.43\cdot10^{0}$
24	$2.58\cdot10^{-3}$	$3.65\cdot10^{-3}$	$2.02\cdot10^{-2}$	$3.79\cdot10^{-2}$	$1.87\cdot10^{-1}$	$5.94\cdot10^{-1}$
32	$1.28\cdot10^{-5}$	$1.77\cdot10^{-5}$	$2.11\cdot10^{-3}$	$2.69\cdot10^{-3}$	$4.20\cdot10^{-2}$	$1.24\cdot10^{-1}$

Table VI. Numerical results for example (4) with polar coordinates.

	$k=1$		$k=2$		$k=3$	
N	E_2	E_∞	E_2	E_∞	E_2	E_∞
8	$1.10\cdot10^{-2}$	$1.40\cdot10^{-2}$	$1.31\cdot10^{-1}$	$2.31\cdot10^{-1}$	$1.91\cdot10^{-1}$	$4.06\cdot10^{-1}$
16	$2.38\cdot10^{-7}$	$3.64\cdot10^{-7}$	$1.07\cdot10^{-3}$	$1.65\cdot10^{-3}$	$1.63\cdot10^{-2}$	$4.15\cdot10^{-2}$
24	$2.97\cdot10^{-11}$	$3.39\cdot10^{-11}$	$2.42\cdot10^{-6}$	$3.00\cdot10^{-6}$	$1.22\cdot10^{-3}$	$2.16\cdot10^{-3}$
32	$2.48\cdot10^{-12}$	$8.23\cdot10^{-12}$	$3.59\cdot10^{-9}$	$4.15\cdot10^{-9}$	$1.65\cdot10^{-6}$	$1.06\cdot10^{-5}$

Table VII. Numerical results for example (5) with polar coordinates.

References

[1] Bernardi, C. and Karageorghis, A.: Spectral method in a part of a disk. *Numer. Math.* **73**, 265-289(1996)

[2] Birdsall, C.K. and Langdon, A.B.: Plasma Physics via Computer Simulation. McGraw–Hill, New York, 1985

[3] Birney, J. and Tremaine, S.: Galactic Dynamics. Princeton University Press, Princeton, 1987

[4] Canuto, C., Hussaini, M.Y., Quarteroni, A., and Zang, T.A.: Spectral Methods in Fluid Dynamics, Springer Series in Computational Physics, Springer-Verlag, Berlin-Heidelberg-New York, 1989

[5] Chen, H., Su, Y.S., and Shizgal, D.: A direct spectral collocation Poisson solver in polar and cylindrical coordinates. *J. Comp. Phys.* **160**, 453-463(2000)

[6] Eisen, H., Heinrichs, W., and Witsch, K.: Spectral methods and polar coordinate singularities. *J. Comp. Phys.* **96**, 241-257(1991)

[7] Gordon, W.J. and Hall, C.A.: Construction of curvilinear co-ordinate systems and their applications to mesh generation. *Int. J. Numer. Meth. Eng.* **7**, 461-477(1973)

[8] Gordon, W.J. and Hall, C.A.: Transfinite element methods: blending-function interpolation over arbitrary curved element domains. *Numer. Math.* **21**, 109-129(1973)

[9] Gottlieb, D. and Orszag, S.A.: Numerical Analysis of Spectral Methods: Theory and Applications. CBMS-NSF Regional Conference Series in Applied Mathematics No. 26, SIAM, Philadelphia, 1977

[10] Grapperhuis, M.J. and Kushner, M.J.: A semianalytic radio frequency sheat model integrated into two dimensional hybrid model for plasma processing reactors. *J. Appl. Phys.* **81**, 569-577(1997)

[11] Haschke, H. and Heinrichs, W.: Splitting techniques with staggered grids for the Navier–Stokes equations in the 2D case. *J. Comp. Phys.* **168**, 131-154(2001)

[12] Heinrichs, W.: Splitting techniques for the pseudospectral approximation of the unsteady Stokes equations. *SIAM J. Numer. Anal.* **30**, 19-39(1993)

[13] Heinrichs, W.: Splitting techniques for the unsteady Stokes equations. *SIAM J. Numer. Anal.* **35**, 1646-1662(1998)

[14] Heinrichs, W.: Spectral collocation on triangular elements. *J. Comp. Phys.* **145**, 743-757(1998)

[15] Heinrichs, W. and Loch, B.: Spectral schemes on triangular elements. *J. Comp. Phys.* **173**, 279-301(2001)

[16] Huang, W. and Sloan, D.M.: Pole condition for singular problems. *J. Comp. Phys.* **107**, 254-261(1993)

[17] Karageorghis, A.: Conforming spectral methods for Poisson problems in cuboidal domains. *J. Scient. Comput.* **9**, 341-349(1994)

[18] Matsushima, T. and Marcus, P.S.: A spectral method for polar coordinates. *J. Comp. Phys.* **120**, 365-374(1995)

[19] Miller, P.A. and Riley, M.E.: Dynamics of collisionless of plasma sheats. *J. Appl. Phys.* **82**, 3689-3709(1997)

[20] Orszag, S.A.: Spectral methods for problems in complex geometries. *J. Comp. Phys.* **37**, 70-92(1980)

[21] Roth, J.R.: Industrial Plasma Engineering. Inst. of Phys., London, 1995

[22] Serikov, V.V. and Nanbu, K.: Spatio-temporal variations in a three-dimensional DC glow discharge via particle-in-cell simulation. *IEEE Trans. Plasma Sci.* **27**, 84-85(1999)

[23] Shen, J.: Efficient spectral–Galerkin methods III: polar and cylindrical geometries. *SIAM J. Sci. Comput.* **18**, 1583-1604(1997)

Figure

Fig. I. Collocation nodes on the unit disc

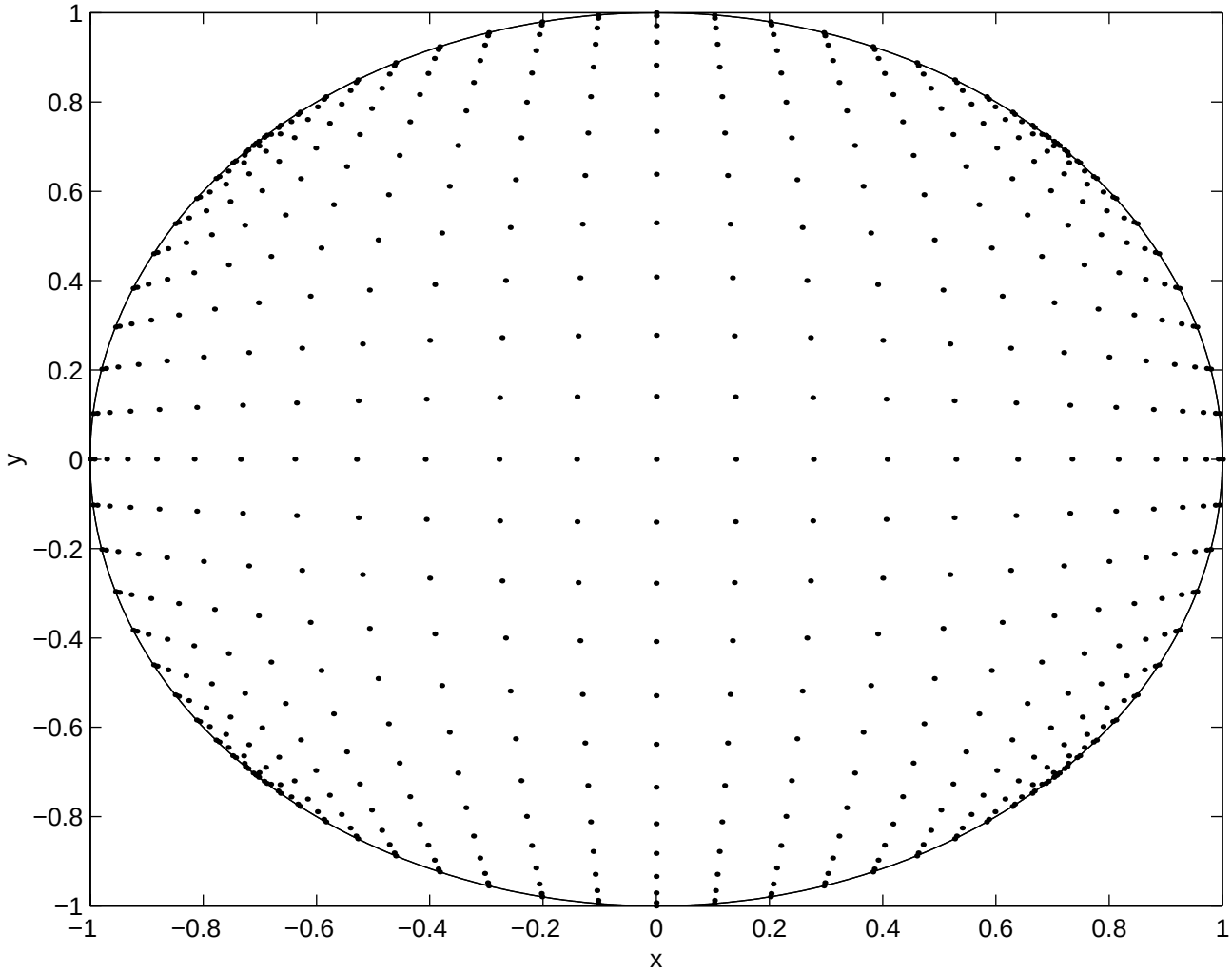

Figure

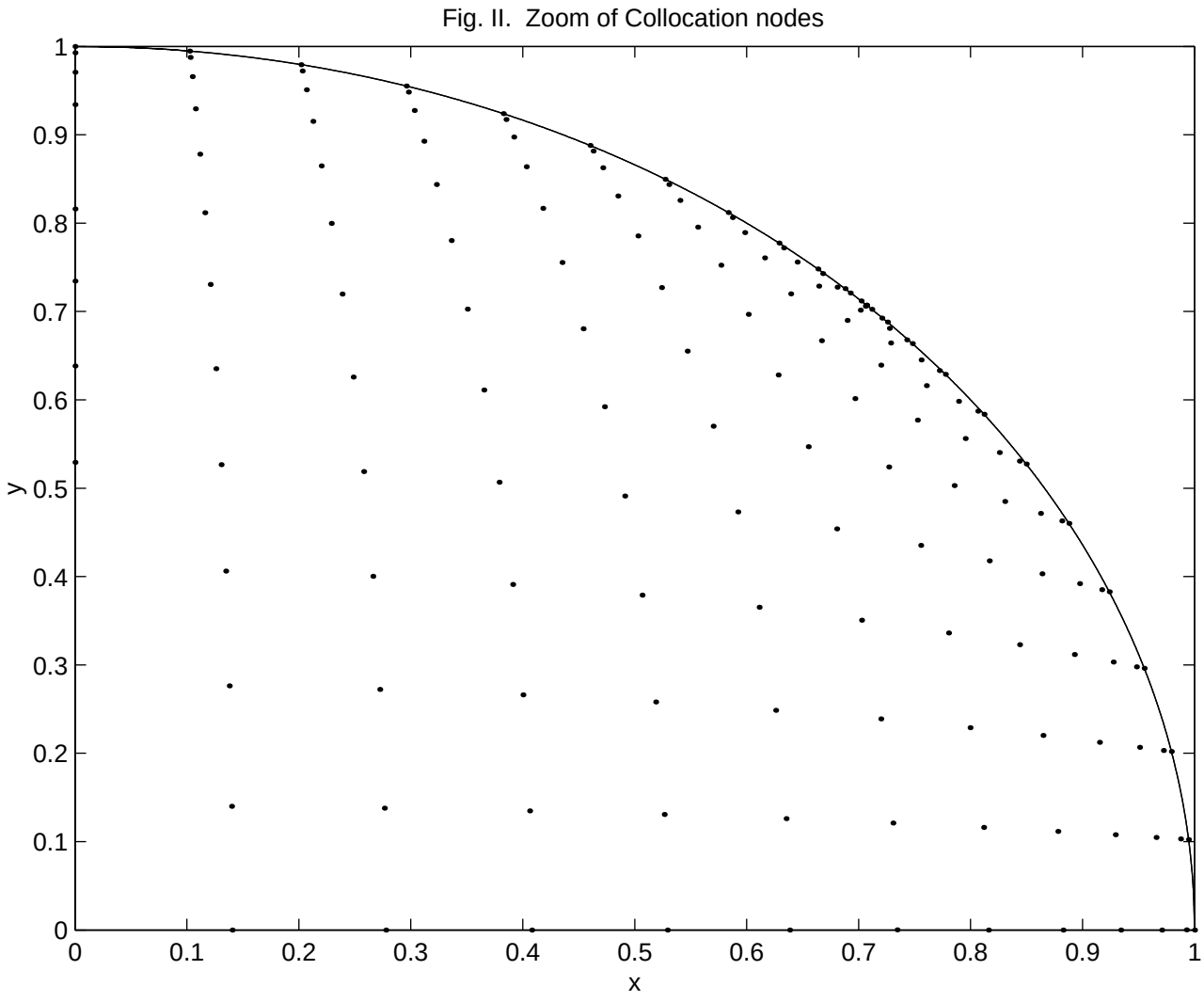

Figure

Fig. III. Collocation nodes on complex geometry (k=1)

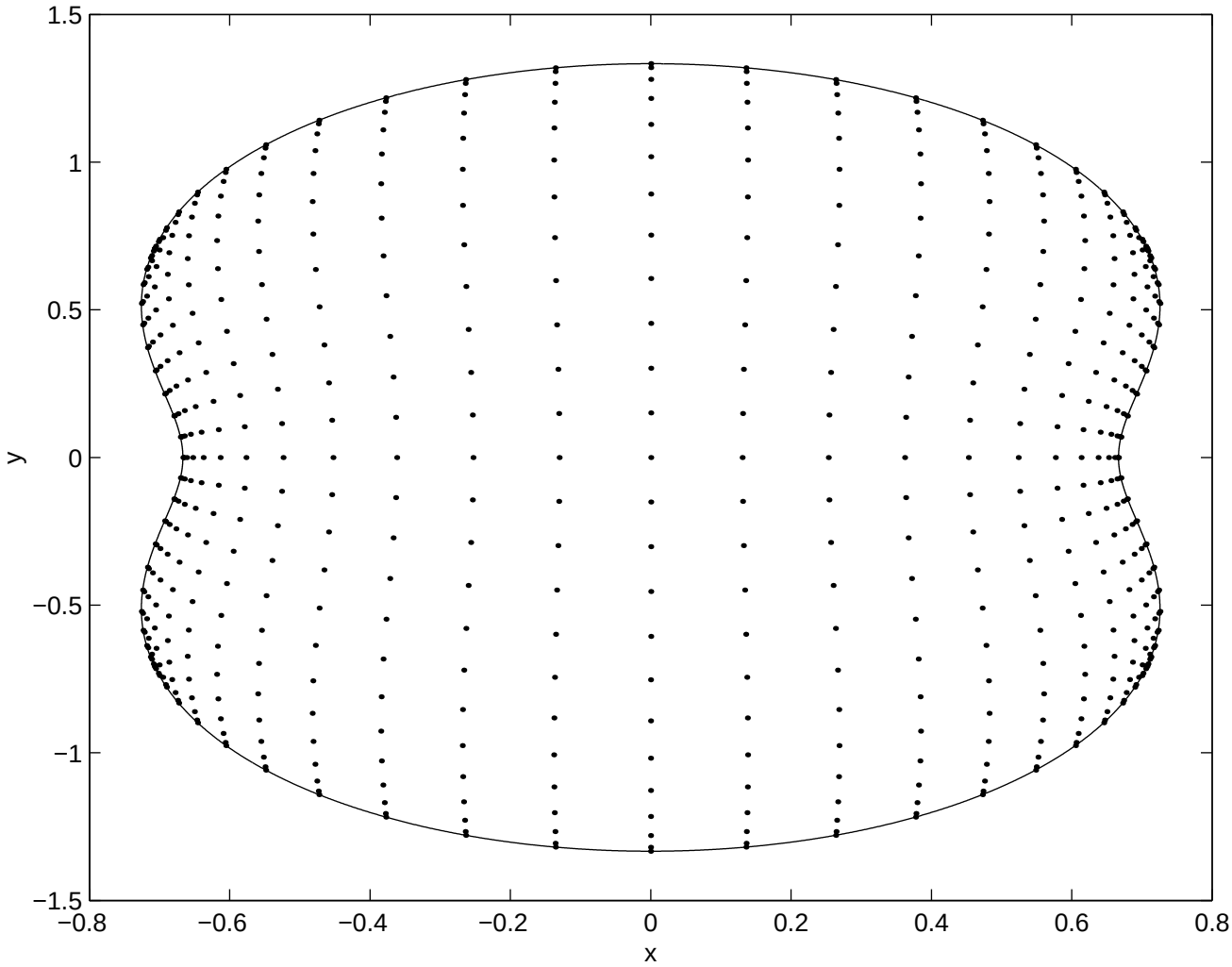

Figure

Fig. IV. Collocation nodes on complex geometry (k=2)

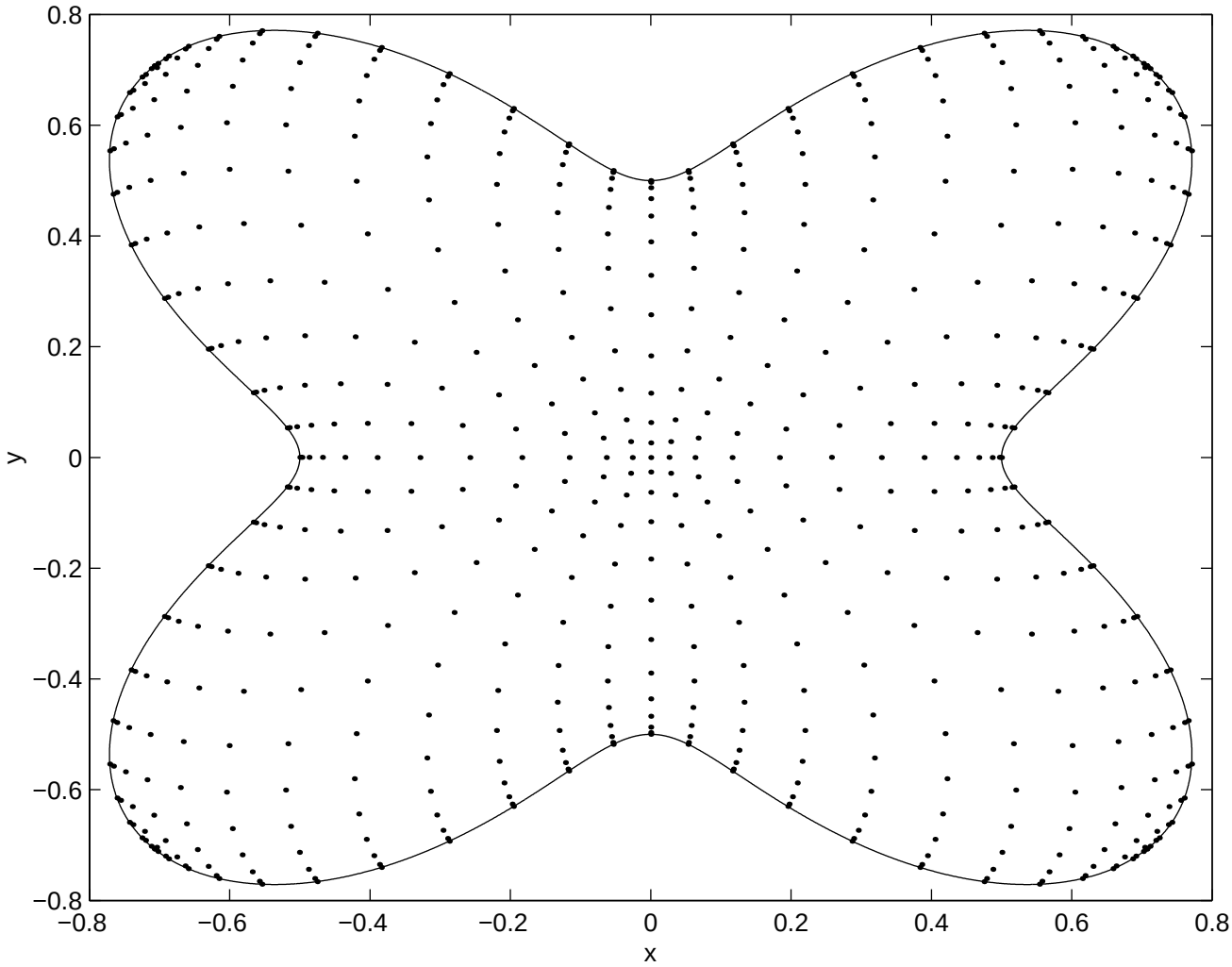

Figure

Fig. V. Collocation nodes on complex geometry (k=3)

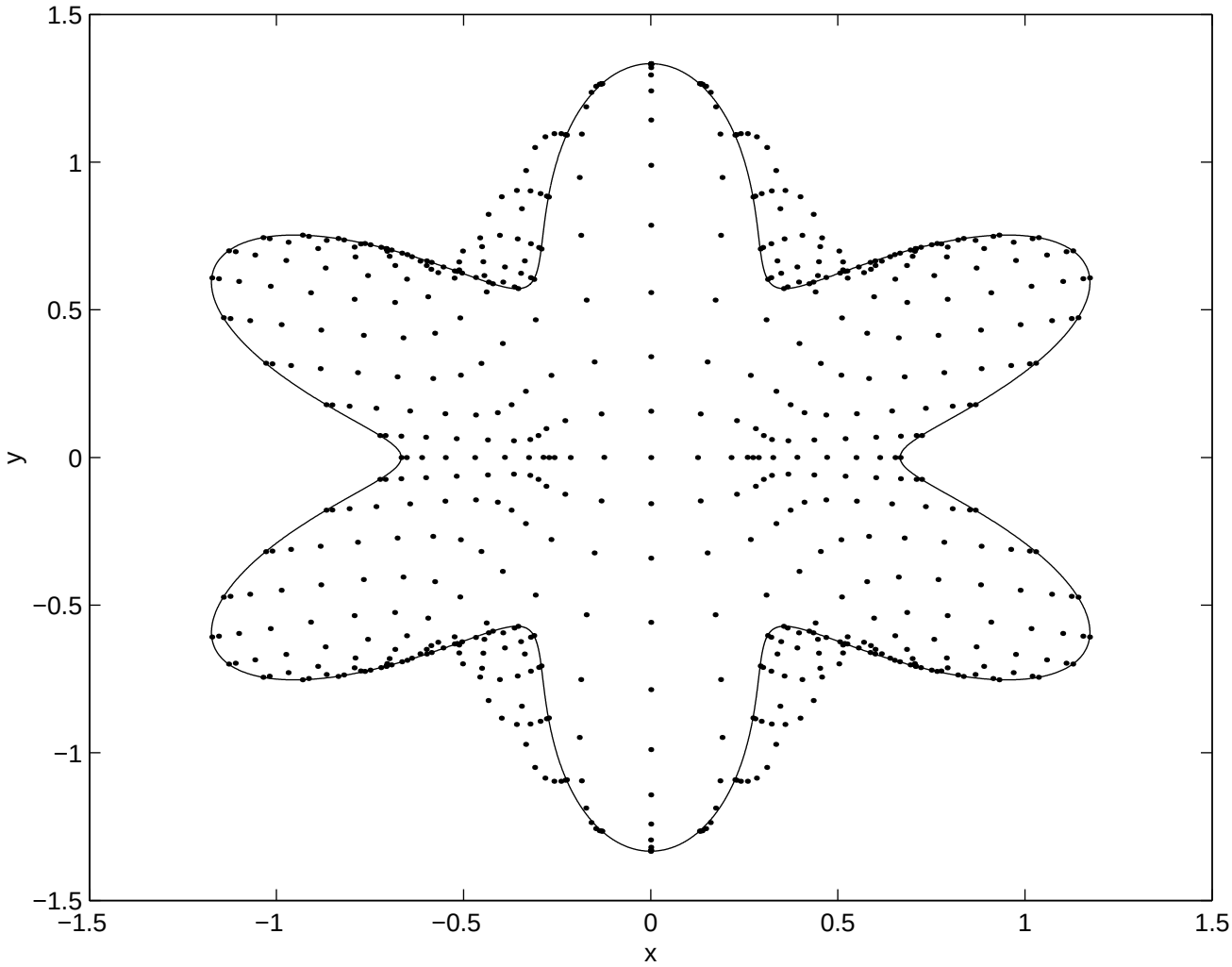

Figure

Fig. VI. Collocation nodes with polar coordinates (k=2)

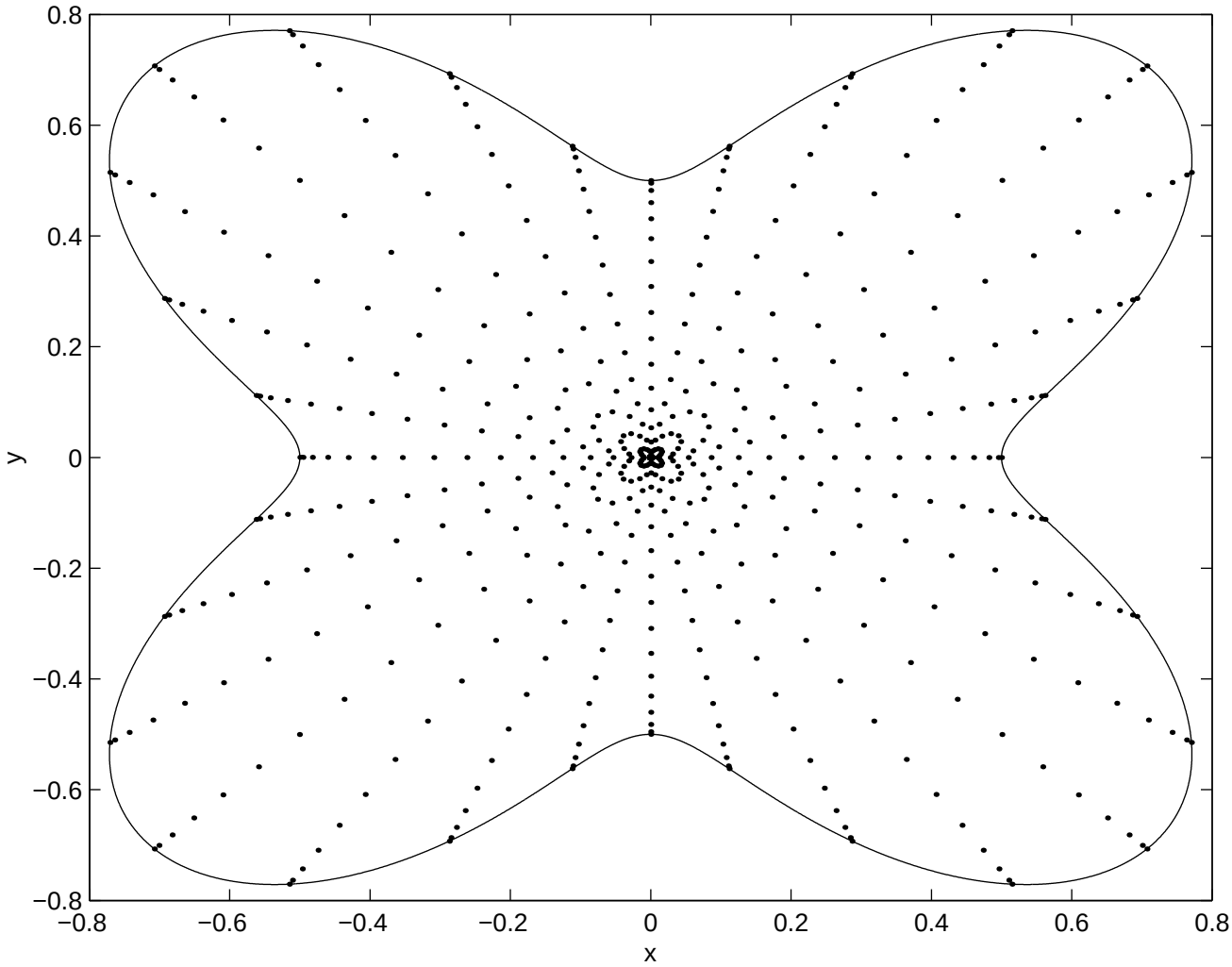

Figure
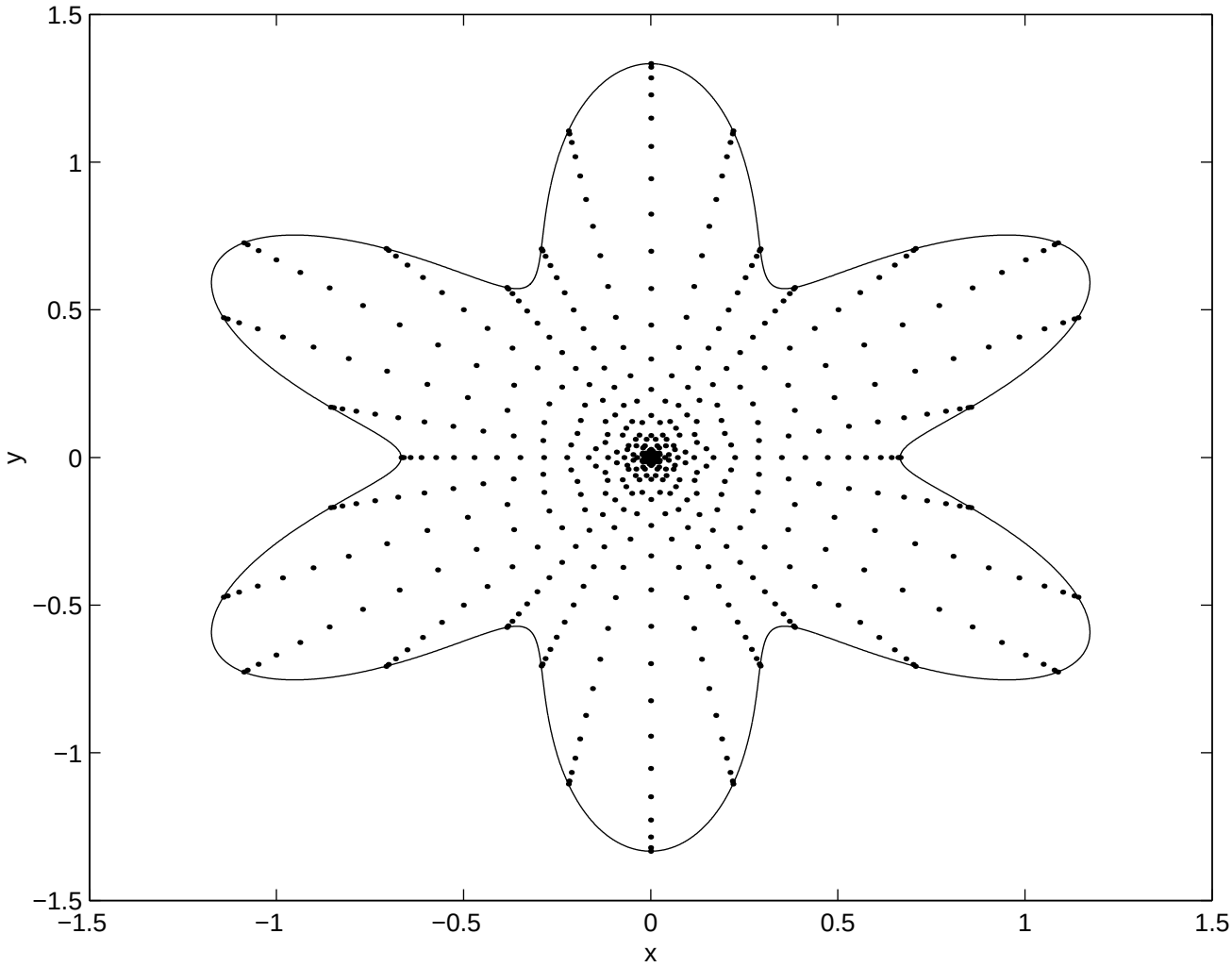
Fig. VII. Collocation nodes with polar coordinates (k=3)